Magnetic circular dichroism and spin polarization in $3d \to 4f$ resonant photoemission from Tb metal in the perpendicular geometry

M. Taguchi,[1,2] G. van der Laan,[1] E. Arenholz,[3] S. S. Dhesi,[1,4] and E. Dudzik[1,5]

[1]*Magnetic Spectroscopy, Daresbury Laboratory, Warrington WA4 4AD, United Kingdom*
[2]*RIKEN/SPring-8, 1-1-1, Mikazuki-cho, Sayo-gun, Hyogo 679-5148, Japan*
[3]*Advanced Light Source, Lawrence Berkeley National Laboratory, Berkeley, California 94720, USA*
[4]*European Synchrotron Radiation Facility, Boîte Postal 220, F-38043 Grenoble, France*
[5]*Hahn-Meitner-Institut, Glienicker Strasse 100, D-14109, Berlin, Germany*

We present combined experimental and theoretical results for the magnetic circular dichroism (MCD) in resonant $4f$ photoemission (RPE) from Tb metal in the perpendicular geometry at different photon energies across the whole of the $M_{4,5}$ resonance. The atomic calculations, which take into account the full multiplet structure and the coherent second-order optical process, give excellent agreement with new experimental results for the resonant photoemission decay. The angular dependence of the MCD-RPE and its strong spin polarization in the M_5 region are also reported. For a single-configuration state the variations in the spectral shape are found to be stronger as a function of angle than as a function of photon energy. Due to the presence of the multiplet structure in the intermediate state $3d^9 4f^9$ the coherent second-order optical process is essential for a correct description of the RPE. While the analysis of the spectra in parallel geometry yields accurate values of the spin-orbit, Coulomb, and exchange interactions, only the angle dependent RPE provides the phase factors of the emitted photoelectron.

I. INTRODUCTION

With the development of high-brilliance synchrotron radiation sources, a plethora of spectroscopies based on polarized x-rays has become available, such as x-ray magnetic circular dichroism (XMCD), x-ray magnetic linear dichroism (XMLD), x-ray natural circular dichroism, x-ray resonant magnetic scattering, to name a few. In these spectroscopies, x-ray absorption spectroscopy (XAS) using circularly polarized radiation, which gives rise to XMCD, has proven to be ideally suited to study the local electronic and magnetic properties of materials since relevant ground-state properties can be determined using powerful sum rules.[1–3] It is well known that this magnetic circular dichroism (MCD) in the absorption spectrum vanishes when the helicity of the incident light is perpendicular to the remanent magnetization direction. However, in this perpendicular geometry (PG) the MCD can still be present in the decay or emission spectrum. Thole, Dürr, and van der Laan[4] observed in PG an MCD in resonant photoemission (MCD-RPE) of 9% for the $2p3p3p$ decay from ferromagnetic nickel. Braicovich *et al.*[5,6] observed that also the MCD in x-ray resonant Raman scattering (RRS) does not vanish for PG. These studies have shown that both MCD-RPE and MCD-RRS can provide information about the core-hole polarization that is not accessible by XMCD. Recent atomic calculations of the MCD-RRS by Fukui *et al.*[7] for the $2p \to 5d$ excitation followed by $3d \to 2p$ radiative decay using a Gd $4f^7$ ground state were in good agreement with experiments on the $Gd_{33}Co_{67}$ amorphous alloy. The authors claimed that the MCD-RRS in PG is caused by cross terms, which are characteristic of the coherent second-order optical process.

Until now, measurements of the MCD-RPE in PG have concentrated on $3d$ transition metals.[4,8–11] Also theoretical investigations on MCD-RPE in PG have been limited to $3d$ transition metals, such as the $2p3p3p$, $2p3p3d$, and $2p3d3d$ decays in Ni metal.[12] For instance, the $2p3p3p$ decay has been analyzed using the atomic process $3d^9 + h\nu \to 2p^5 3d^{10} \leftrightarrow 3p^4 3d^{10} \varepsilon l \leftrightarrow 3s^1 3d^9 \varepsilon l$, where εl denotes a continuum photoelectron state and the photon energy $h\nu$ is tuned across the $2p \to 3d$ resonance. Very recently, Taguchi and van der Laan[13] have used a method based on the coherent second-order optical process to calculate the $2p3p3p$ MCD-RPE in PG from Ni metal. A very good agreement was obtained with the experimental results by taking the wave function of the ejected photoelectron as a superposition of outgoing and incoming spherical waves. The angular dependence of the MCD depends on the phase factors of the outgoing photoelectrons. Therefore, the results indicate the importance of the phase factor of the ejected photoelectron for the angular dependence.

The Ni $2p3p3p$ RPE is a very simple case compared to that of the $4f$ metals. In general the calculations are rather involved and it is normally not possible to simplify the interpretation of the RPE process by dropping some terms in the Hamiltonian. The direct photoemission process from the initial state to the final state, the photon excitation to an intermediate state followed by the decay into the final state, the coherent superposition of these processes and the multiplet-term dependent lifetime effect in the intermediate state are all vital ingredients in the RPE. The combination of these processes determines the photoemission intensity as a function of the incident photon energy, binding energy (BE), geometry (including the angle dependence), light polarization, sample magnetization, and photoelectron spin. Such an evaluation requires considerable computational effort which

has certainly limited the use of this spectroscopy up to now. The comparison between theory and experiment as a function of all these experimental parameters, that can be either varied or measured, provides a much more stringent test than standard RPE. It can also avoid errors in the interpretation of the experiment, because while conventional calculations often make simplifying assumptions, such as angular integration, these conditions are in practice not fulfilled since photoelectrons are always detected within a restricted angular acceptance cone, hence the mentioned phase factors will influence the observed spectra. Moreover, it has been demonstrated that by applying the sum rules for angle-dependent MCD-RPE (Refs. 4,12) and MCD-RRS (Refs. 6,14) it is possible to extract higher order ground-state spin and orbital coupled multipole moments, such as the octupolar and hexadecapolar moments. Measurement of the MCD in PG has in this case the advantage that the isotropic contribution drops out. This method is complementary to the sum rule analysis for XAS that provides the number of valence holes and the spin-orbit interaction,[15] for XMCD that provides the spin and orbital magnetic moments,[1–3] and for XMLD that provides the quadrupole moment and the magnetic anisotropy.[16]

The $M_{4,5}$ XAS,[17] the $4f$ photoemission[18] and the RPE (Ref. 19) spectra of rare earths systems all show a large multiplet structure and a strong MCD.[20,21] Although the analysis of these spectra provides accurate values of the spin-orbit, Coulomb, and exchange interactions,[17] it is only the angle-dependent RPE that can be used to test the phase factors of the emitted photoelectron. Incorporation of the coherent second-order optical process is essential for a correct treatment of the angle-dependent RPE in the presence of multiplet structure in the intermediate state. Using the angle dependent Tb $3d \rightarrow 4f$ RPE as a critical test for the coherent second-order model calculations, we find a very good agreement with experimental results. On the other hand, a simplified model based on the fast-collision approximation would break down due to the multiplet structure. In this model one assumes that the intermediate state lifetime is so short (i.e., the energy broadening Γ of the intermediate state lifetime is sufficiently large) that there are no scattering paths from the initial to the final states with an energy difference more than Γ.

This paper is organized as follows. The experimental details are described in Sec. II. The theoretical model and formalism are given in Sec. III. The calculated results and comparison with experimental results is presented in Sec. IV, where also the angle dependence and the spin polarization are discussed. Conclusion are drawn in Sec. V.

II. EXPERIMENTAL

Tb(0001) films with a thickness of 10 nm were epitaxially grown on W(110) following a standard procedure.[22] The films were in-plane magnetized using a nearby solenoid inside the UHV chamber. Measurements were performed on the *in situ* prepared samples, in remanent magnetic state and at a temperature of 30 K, using circularly polarized x rays from the undulator beam line ID12B (currently ID08) at the European Synchrotron Radiation Facility (ESRF). This beam
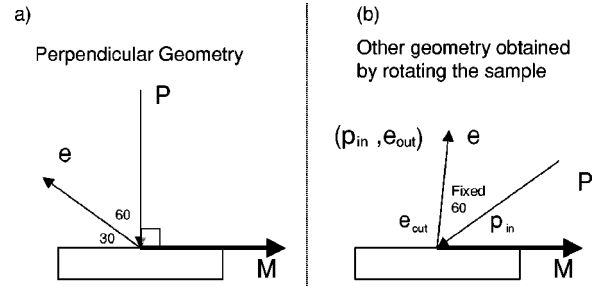

FIG. 1. Experimental geometry for the MCD-RPE where **P** is the direction of the incident circularly polarized x rays, **M** the remanent magnetization direction, and **e** the direction of the detected photoelectrons. The angle $\angle$**e,P** is fixed to 60°. (a) Perpendicular geometry (PG); (b) Geometry for measuring the angular dependence, where the angle $p_{in} = \angle$**P,M** is varied.

line was equipped with a spherical grating monochromator giving soft x rays with an energy resolution of ~ 0.4 eV and a degree of circularly polarization of $85 \pm 5\%$ in the region of interest.

The geometry for photoemission is depicted in Fig. 1, where **M** is the remanent magnetization direction and **P** the direction of the incident x rays, which is parallel to the helicity vector. Photoelectrons were collected around the direction **e** using a hemispherical energy analyzer with an acceptance cone of 20° and an energy resolution of 0.2 eV. The large acceptance angle for the photoelectrons ensures the averaging over diffraction effects which give variations on a scale of a few degrees. Due to the experimental constraints in ultrahigh vacuum the angle $\angle$**P,e** is fixed to 60°. Figure 1(a) shows the PG, where **P**$\perp$**M**. Figure 1(b) shows the geometry used for the angle-dependent measurements, where the sample is rotated around the axis **P**$\times$**e**, thereby varying the angle $p_{in} = \angle$**P,M**. Since the magnetic remanence of the Tb film is notoriously in-plane we could not reach the **P**$\|$**M** alignment and instead used a grazing angle of $p_{in} = 30°$ as done also in Ref. 19.

The spectra were normalized to the incident photon flux and an integral background correction was performed for the spectra measured with + and − helicity prior to taking the MCD difference spectrum. Details of this procedure have been described previously.[19] No saturation corrections were applied.

The XAS and XMCD spectra were recorded in total-electron yield. The Tb $M_{4,5}$ XMCD measured for $p_{in} = 30°$ (Fig. 2) was the same as reported previously.[19] Prior to taking the data for the MCD-RPE in PG (Fig. 3) it was verified that the XMCD signal was completely zero in this geometry.

III. THEORY

Our aim in this study is to calculate the $3d \rightarrow 4f$ XAS, XMCD, and the MCD-RPE across the $3d \rightarrow 4f$ excitation for a $4f^n$ system in spherical symmetry. We assume that for the rare earths the interaction with the band like $(5d6s)^3$ is so small that its influence can be neglected. We consider the excitation-decay process $4f^n + h\nu \rightarrow 3d^9 4f^{n+1} \leftrightarrow 4f^{n-1} \varepsilon l$ in resonance with the direct photoemission process $4f^n + h\nu$
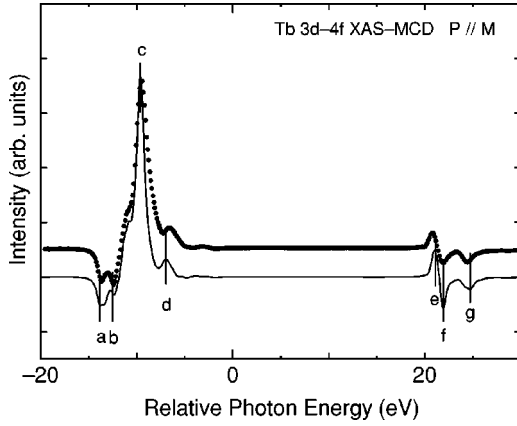
FIG. 2. Calculated Tb $M_{4,5}$ XMCD for $\mathbf{P}\|\mathbf{M}$ (draw line) together with the experimental spectrum (closed symbols) for $\angle\mathbf{P},\mathbf{M}$ $=30°$. The shape of the XMCD is not expected to be angle dependent. The photon energies at which the resonant photoemission spectra have been taken are marked by $a, \ldots, g$.

$\rightarrow 4f^{n-1}\varepsilon l$, where $h\nu$ is the incident photon energy, and $4f^{n}$, $3d^{9}4f^{n+1}$, and $4f^{n-1}\varepsilon l$ are the electronic configurations of the ground state, intermediate state, and final state, respectively. In the calculation the kinetic energy of the continuum electron is taken such that the total energies of the $3d^{9}4f^{n+1}$ and $4f^{n-1}\varepsilon l$ are the same, in fact these configurations form the same coherent state.

The method for calculating the RPE is almost the same as Ref. 23 and leads to the same results for parallel geometry as Ref. 19. The Hamiltonian can be written as

$$H = H_0 + V_r + V_a, \qquad (1)$$

where H_0 describes the atomic configuration including Coulomb, exchange and spin-orbit interactions of the $3d$ and $4f$ shells in the presence of a magnetic field, V_r is the radiative dipole transition of $3d \rightarrow 4f$ and $4f \rightarrow \varepsilon l$, and V_a is the Auger transition with radial matrix elements $R(3d,\varepsilon l;4f,4f)$.

The spectrum of the RPE is given as

$$F(\varepsilon, h\nu) = \sum_{k,\beta} |\langle k\beta|V_r + V_a G(h\nu)T|g\rangle|^2$$

$$\times \delta(h\nu + E_g - E_{k\beta})\delta(\varepsilon - \varepsilon_k), \qquad (2)$$

where

$$G(h\nu) = \frac{1}{h\nu + E_g - H_0 + i\Gamma}, \qquad (3)$$

where we take into account V_r up to the first order and V_a up to the infinite order. ε is the photoelectron energy, $|g\rangle$ the ground state of H_0 with energy E_g, and $|k\beta\rangle$ the final states with energies $E_{k\beta}$. As usual, we ignore the interaction between the emitted photoelectron and the ionic configuration, so that the final states $|k\beta\rangle$ and their energies can be decoupled as $|k\beta\rangle = |k\rangle|\beta\rangle$ and $E_{k\beta} = \varepsilon_k + E_\beta$, respectively, where $|k\rangle$ represents the εl continuum electron state with energy ε_k, and $|\beta\rangle$ the final states of the Tb ion with energy E_β.

The operator T, called the t matrix, represents the effective transition from $|g\rangle$ to the intermediate states $|m\rangle$ and is defined as

$$\langle m|T|g\rangle = \langle m|V_r|g\rangle - i\pi \sum_{k,\beta} \langle m|V_a|k\beta\rangle\langle k\beta|V_r|g\rangle$$

$$\times \delta(h\nu + E_g - E_{k\beta}). \qquad (4)$$

The lifetime operator Γ is defined as

$$\langle m|\Gamma|m'\rangle = \sum_{k,\beta} \langle m|V_a|k\beta\rangle\langle k\beta|V_a|m'\rangle \delta(h\nu + E_g - E_{k\beta}). \qquad (5)$$

The wave function of the ejected photoelectron in the continuum state travelling in the direction $\hat{k}$ with energy ε_k is given by

$$|\mathbf{k}\rangle = \frac{1}{k} \sum_{l,m} i^l e^{-i\delta_l} Y_{lm}^*(\hat{k}) R_{\varepsilon_k l}(r) Y_{lm}(\hat{r}), \qquad (6)$$

where δ_l is the total phase shift of the lth partial wave and $R_{\varepsilon_k l}(r)$ is the radial part, and the spherical harmonics Y_{lm} have the Condon and Shortley phase convention.[24] Substitution of Eq. (6) into Eq. (2) can lead to interference between spherical harmonics with different l values. The angular dependent MCD spectrum will be sensitive to the phase factors of the photoelectron.

$F(\varepsilon, h\nu)$ gives a two-dimensional distribution of the photoemission. By slicing F along the binding energy (BE $= h\nu - \varepsilon$) for fixed $h\nu$ we obtain the RPE spectra, which give the $4f$ energy distribution. By slicing F along $h\nu$ for fixed BE we obtain the constant-initial state (CIS) spectra (not used in this paper). The integration of F over the emitted electron energy ε (i.e. summing over the CIS spectra) gives the $M_{4,5}$ XAS, and hence the XMCD.

IV. RESULTS AND DISCUSSION

We calculated the Tb $M_{4,5}$ XMCD in parallel geometry ($\mathbf{P}\|\mathbf{M}$) and the MCD-RPE for different angles. The atomic Slater integrals, spin-orbit interaction, electric-dipole transition probabilities and Auger matrix elements were obtained using Cowan's Hartree-Fock program with relativistic corrections.[25] The calculated values are listed in Ref. 19. The Slater integrals $F^k(4f,4f)$, $F^k(3d,4f)$, and $G^k(3d,4f)$ were scaled to 84, 100, and 80 %, respectively, as obtained from optimizing the Tb $M_{4,5}$ XMLD,[21] off-resonant photoemission,[22,26] and $3d4f4f$ MCD-RPE.[19] Although the scaling influences the relative energy positions of the multiplet peaks, its effect on the relative peak intensities in the MCD spectrum is small. Therefore, the effect of this scaling has not much consequences for the purpose of the present work. The allowed symmetry for the orbital quantum number of εl is $l = d, g$ for direct photoemission (dipole transitions) and $l = s, d, g, i, l$ for the Auger process (Coulomb interaction). We will neglect the l channel which contributes the largest matrices in the calculation but makes little difference for the total intensity. The calculated Hartree-Fock values of
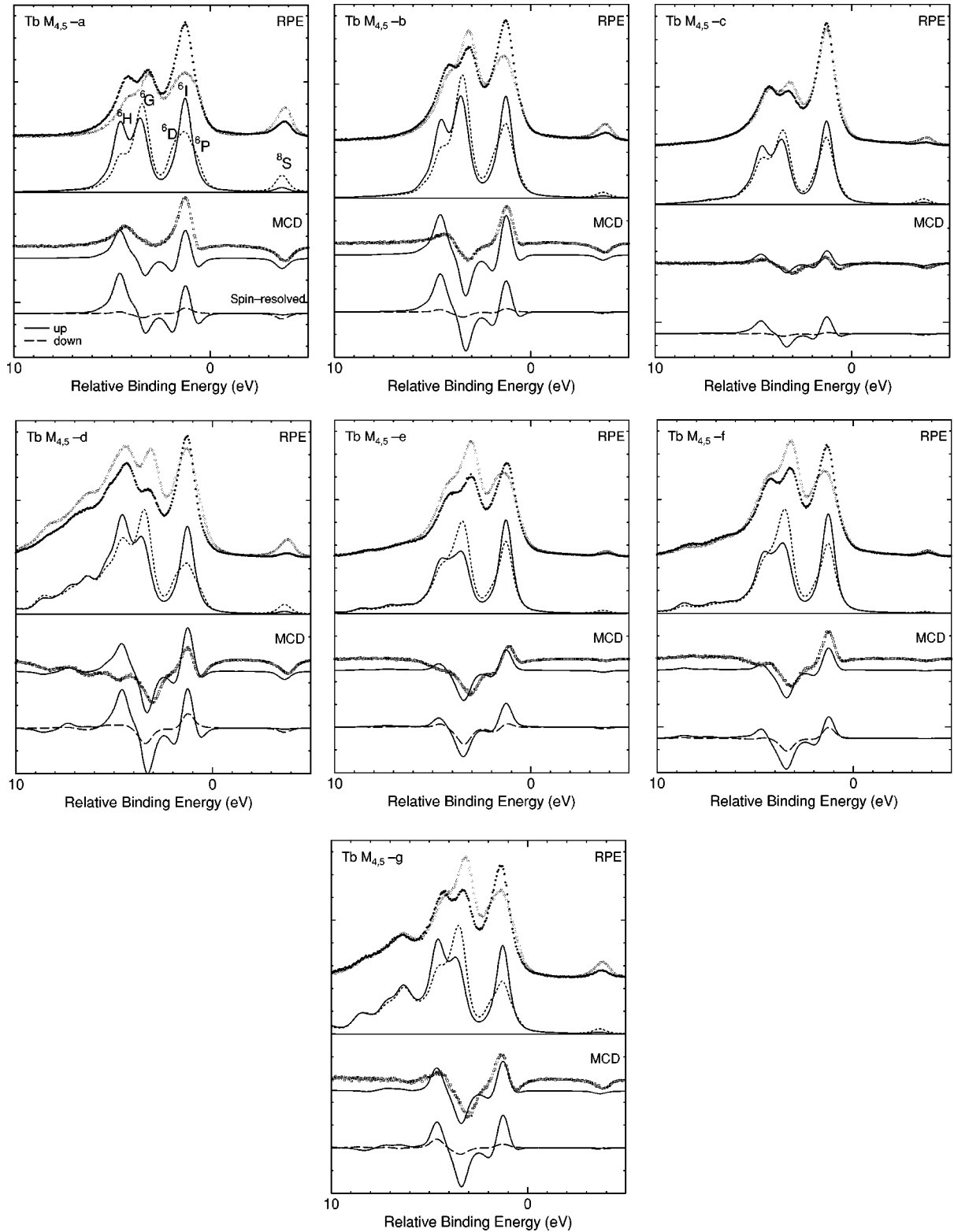
FIG. 3. Tb $3d \rightarrow 4f$ resonant photoemission (RPE) and corresponding MCD spectra in perpendicular geometry [see Fig. 1(a)] at the photon energies marked by $a, \ldots, g$ in the $M_{4,5}$ XMCD spectrum of Fig. 2. Upper panels: calculated RPE for $+$ helicity (drawn line) and $-$ helicity (dashed line) of the incident x rays together with the experimental results for $+$ helicity (closed symbols) and $-$ (open symbols) helicity. Middle panels: calculated MCD spectra (drawn line) and experimental results (open squares). Lower panels: calculated spin polarized MCD spectra: $I_{\mathrm{MCD,up}}$ (drawn line) and $I_{\mathrm{MCD,down}}$ (dashed line).

the phase shifts δ_s, δ_d, δ_g, and δ_i with respect to δ_l were 4.32, 1.76, 4.62, and 5.81 rad, respectively, for a kinetic energy of ~ 1250 eV. For the $4f^7$ final states we took a lifetime broadening of $\Gamma = 0.17$ eV and a Gaussian broadening due to the experimental resolution of $\sigma = 0.085$ eV.[18] For comparison with the experiment, Γ_0 was taken as 0.4 eV for the $M_{4,5}$ edges. The calculated RPE spectra were fitted using an effective Stokes parameter of $S_3 = 0.8$, which takes into account the degree of circular polarization of $85 \pm 5\%$ and the incomplete magnetic saturation.

Figure 2 shows the calculated Tb $M_{4,5}$ XMCD in parallel geometry, which is in good agreements with experimental results and with previous atomic calculations.[19] The Tb ground state $^7F_6$ ($\sim 95\%$ purity in intermediate coupling) has total angular momentum $J = 6$ and is connected with the intermediate states J' via the dipole selection rules $\Delta J = 0$, ± 1 where $J' = 5$ gives positive features (c, d, e) and $J' = 7$ negative features (a, b, f, g) in the XMCD.

A. Perpendicular geometry

1. MCD-RPE

The calculated results for the RPE in PG [see Fig. 1(a)] are shown in the upper panels of Fig. 3, where the spectra for $h\nu = a, \ldots, g$ are obtained by tuning the photon energy to the corresponding peaks a to g in the $M_{4,5}$ XMCD of Fig. 2. The experimental spectra are shown by open (closed) symbols and the theoretical spectra by dashed (drawn) curves for the $-$ ($+$) helicity of the incident x rays. The calculated results are in very good agreement with the experiment for all photon energies. As was already pointed out for angle-integrated RPE,[19] the lower BE region (below -2 eV) contains a single peak arising from the ^8S state. The region between 0 and 3 eV contains the $^6P, ^6I$, and ^6D states and the region between 3 and 6 eV contains mainly ^6G and ^6H states. For each photon energy the sextet spin states display strong signals, while the octet spin state (^8S) is rather weak. On the other hand, for $h\nu = d$ and g the high BE region (above 6 eV) shows a rather strong contribution from quartet spin states, because the corresponding peaks in the XMCD contain a relatively high amount of states with lower spin character, such as 41% quintet and 53% triplet spin states, respectively.

The middle panels in Fig. 3 show the corresponding MCD-RPE in PG. For $h\nu = c$, e, f, and g, there is a good agreement between the calculated (drawn) and experimental (dashed) spectra, but there are some differences for $h\nu = a$, b, and d. For $h\nu = a$, the ^6G and ^6D are negative in the calculation but appear as slightly positive in the experiment. For $h\nu = b$, all multiplet states have the correct sign but the calculated ^6G, ^6H, and ^6D are quite a bit larger than in the experiment. For $h\nu = d$, the ^6H gives a large positive signal in the calculation, but is slightly negative in the experiment. In the calculation the intensity at the high BE side is higher than in the experiment and also the energy positions of the peaks are slightly higher. Such a reduction in intensity and shift toward higher BE has also been observed for other core-level photoemission spectra.[19,21,27]

2. Systematics

We shall now make a comparison between the spectral shapes of MCD at different $h\nu$. For this purpose we look at the calculated spectra. The spectral variations as a function of angle are more smooth in the experiment than in the theory, because the former were done using a photoelectron detector with an acceptance cone of $20°$, whereas in the latter the precise emission angle was used.

According to Ref. 19, for parallel geometry the $J' = 5$ (positive XMCD) gives intense peaks for high L values in the MCD-RPE, while $J' = 7$ (negative XMCD) gives intense peaks for low L values. Since the XMCD signal varies strongly with $h\nu$ (Fig. 2) there will be strong variations in the MCD-RPE spectral shape in parallel geometry for small changes in $h\nu$. On the other hand, judging from Fig. 3, such strong variations do not seem to be present in the case of the PG, where the signature of the MCD-RPE is quite similar for every photon energy. Figure 3 shows that peaks with high L values (^6H and ^6I) are positive while those with lower L values ($^8S, ^6P, ^6D$, and ^6G) are negative. The MCD in PG is usually strongest for the highest L values, i.e., $^6G, ^6H$, and ^6I and becomes weaker for lower L values.

3. Spin dependence

It is also of interest to consider the spin-polarization of the emitted photoelectron for MCD-RPE in PG.[28] The lower panels of Fig. 3 show for different $h\nu$ the calculated spin-polarized MCD spectra, which are defined as

$$I_{\text{MCD,up}} = I_{+,\text{up}} - I_{-,\text{up}},$$

$$I_{\text{MCD,down}} = I_{+,\text{down}} - I_{-,\text{down}}.$$

For all photon energies we find a strong spin polarization of the MCD-RPE with mainly spin-up photoemission for the low-spin (sextet) states and spin-down photoemission for the high-spin (^8S) state. This is due to the selection rule, $\Delta S = s = \pm \frac{1}{2}$, from the septet spin ground state, where s is the spin of the photoelectron. The large spin polarization can also be appreciated from the spin polarized spectra

$$I_{\text{up}} = I_{+,\text{up}} + I_{-,\text{up}},$$

$$I_{\text{down}} = I_{+\text{down}} + I_{-,\text{down}},$$

which are shown in Fig. 4. The strong spin polarization arises because the Tb has 6.94 spin-up $4f$ electrons but only 1.06 spin-down $4f$ electron.[26]

The MCD spectrum can be decomposed as

$$I_{\text{MCD}} = I_{\text{MCD,up}} + I_{\text{MCD,down}}$$
$$= I_{+,\text{up}} - I_{-,\text{up}} + I_{+,\text{down}} - I_{-,\text{down}},$$

and a comparison with the spin spectra in Fig. 3 shows that there is a strong resemblance between the I_{MCD} and the $I_{\text{MCD,up}}$ spectrum. This is due to the fact that the $I_{\text{MCD,down}}$ specrum is small.
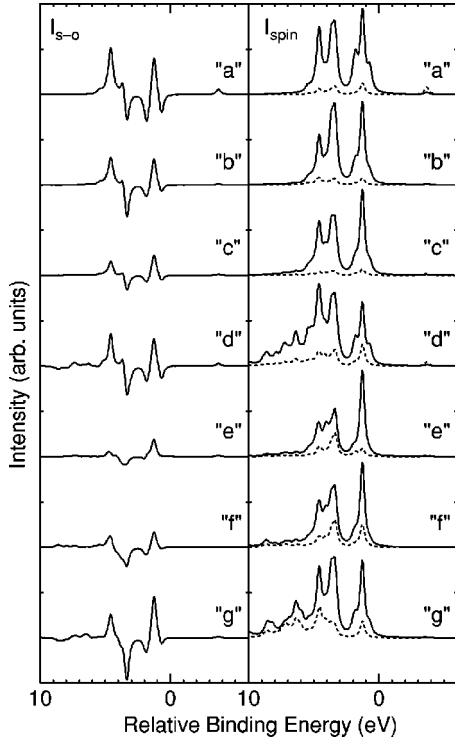
FIG. 4. Tb $3d \rightarrow 4f$ RPE in PG for the different photon energies across the $M_{4,5}$ resonance. Left panel: I_{s-o}; right panel: I_{up} (drawn line) and I_{down} (dashed line).

Figure 4 further shows the spin-orbit spectrum, which measures an alignment between the spin and orbital moments of the $4f$ hole created in the final state, and which is defined as[26]

$$I_{s-o} = I_{MCD,up} - I_{MCD,down} = I_{+,up} - I_{-,up} - I_{+,down} + I_{-,down},$$

which is also quite similar to the I_{MCD} with, as expected, a reversed sign for the ^8S peak.

B. Angular dependence

1. Calculated results

While the ^8S peak in the MCD-RPE has a rather low intensity in PG [Fig. 3(a)], in the study for the parallel geometry[19] this state has a rather large negative intensity, especially for $h\nu=a$. In order to be able follow the variations in spectrum in going from parallel geometry to PG, we plotted for different angles p_{in} in Fig. 5 the RPE for $h\nu=a$ and b, for $-$ and $+$ helicity. The angle $\angle \mathbf{P},\mathbf{M}$ is fixed at 60° [Fig. 1(b)], so that the "parallel geometry" of Ref. 19 corresponds to $p_{in}=30°$, $e_{out}=90°$, while PG corresponds to $p_{in}=90°$, $e_{out}=30°$.

For $h\nu=a$ the ^8S state has a large intensity for $-$ helicity resulting in a strong MCD signal at $p_{in}=30°$ [Fig. 5(a)]. Going to 90°, the ^8S decreases strongly for $-$ helicity and also the ^6P, ^6I, and ^6D decrease slightly for both helicities. On the other hand, the ^6G and ^6H increase for both helicities. In the MCD spectra [Fig. 5(b)] the negative peak of the ^6P decreases in going to PG in the same way as the ^8S, while the ^6H shows the opposite behavior. The ^6I, ^6D, and

^6G do not change very much.

For $h\nu=b$ and $p_{in}=30°$ [Fig. 5(b)] the ^6I is large for $+$ helicity while the ^8S is relatively small. The angle dependence of the ^8S and ^6H is the same as for $h\nu=a$, but the ^6P shows no angle dependence while the ^6D and ^6G increase in going to PG.

2. Comparison with experiment

Figures 6 and 7 show for $h\nu=c$ and d, respectively, the comparison between the calculated (left panels) and the experimental (right panels) angle dependence, where (a) shows the RPE for the two helicities and (b) the resulting MCD. For $h\nu=c$ [Fig. 6(b)] the MCD shows an excellent agreement between theory and experiment. For $p_{in}=30°$, the signal is largest for $+$ helicity over the whole BE region, except for the ^8S which is larger for $-$ helicity. Going towards 90°, the intensity for $-$ helicity increases, which makes the spectral shape more similar for both helicities and the ^6G finally reverses at 90°. The ^8S is always negative and increases in going to 90°. The ^6I has always a positive MCD but decreases for increasing p_{in}.

For $h\nu=d$ the comparison between theory and experiment for the RPE and MCD is shown in Figs. 7(a) and 7(b), respectively. Also in this case the agreement is quite good. As anticipated above, the quartet states at the higher BE side have a large intensity. The RPE shows an angle dependence of the quartet states but this is not so visible in the MCD.

V. CONCLUSIONS

We have presented experimental results for the magnetic circular dichroism in Tb $3d \rightarrow 4f$ resonant photoemission (MCD-RPE) in perpendicular geometry (PG). These results have been compared with calculations using an atomic model that takes into account the full multiplet structure and the coherent second-order process. Very good agreement between the experimental results and the calculations is obtained for the RPE and corresponding MCD. The presented calculations show that the MCD-RPE in PG can be successfully exploited in complicated cases, such as the rare earth systems, and not only in the more simpler cases explored up to now. While the strong variations in the XMCD signal as a function of photon energy lead to equally strong changes in the spectral shape of the MCD-RPE in the parallel geometry, this is not the case in PG, where the signature of the MCD-RPE is quite similar for the different photon energies across the absorption edge. The MCD in PG is usually the strongest for the highest L values, i.e., ^6G, ^6H, and ^6I, and becomes weaker for lower L values. On the other hand, as shown in Ref. 13, strong spectral changes with incident photon energy are expected when the final state is a mixture (hybridization) of different electronic configurations. This could open up an interesting method to study hybridization effects.

While the RPE in parallel geometry has been well understood in terms of spin-orbit, Coulomb, and exchange interactions,[19] only the angle dependent RPE can verify the phase factors of the emitted photoelectron. We have also presented calculations which show that the MCD in RPE is strongly spin polarized. This is due to the fact that the
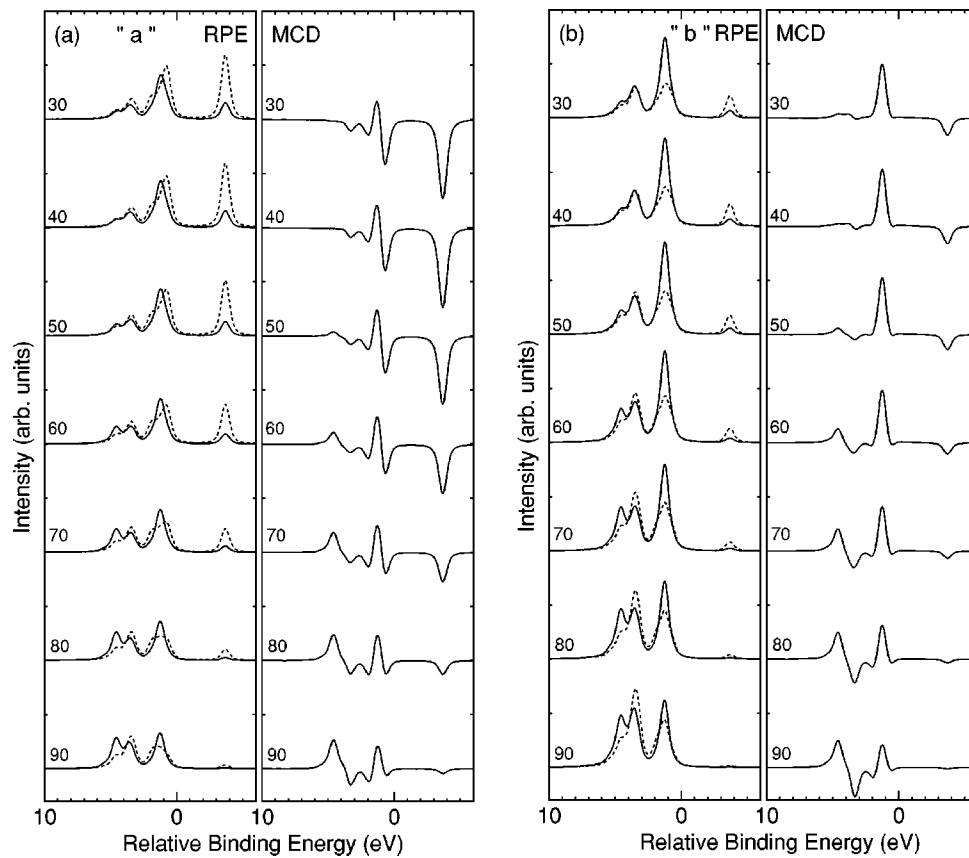
FIG. 5. Calculated Tb $3d{\rightarrow}4f$ RPE at different angles for (a) $h\nu{=}a$ and (b) $h\nu{=}b$. The experimental geometry is as in Fig. 1(b) with the angle p_{in} indicated for each spectrum. Left panels: RPE for $+$ helicity (drawn line) and $-$ helicity (dashed line) of the incident photon; right panels: resulting MCD.
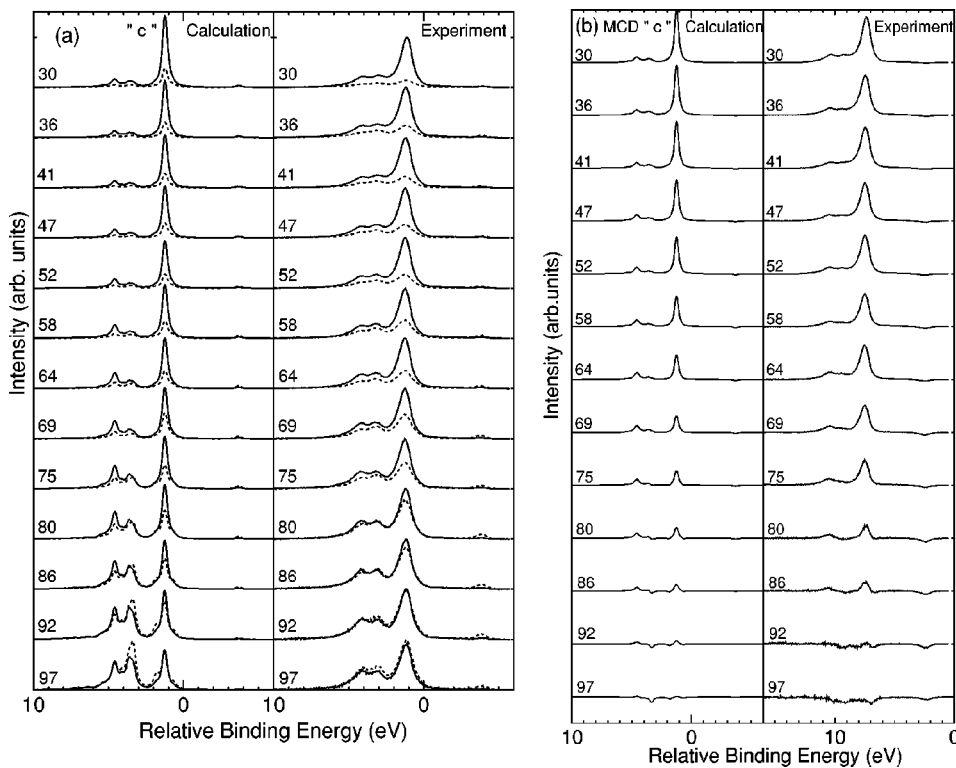

FIG. 6. Tb $3d{\rightarrow}4f$ RPE at different angles for $h\nu{=}c$. The geometry is as in Fig. 1(b) with p_{in} indicated for each spectrum. (a) RPE for $+$ helicity (drawn line) and $-$ helicity (dashed line); (b) resulting MCD. Left panels: calculation; right panels: experimental results.
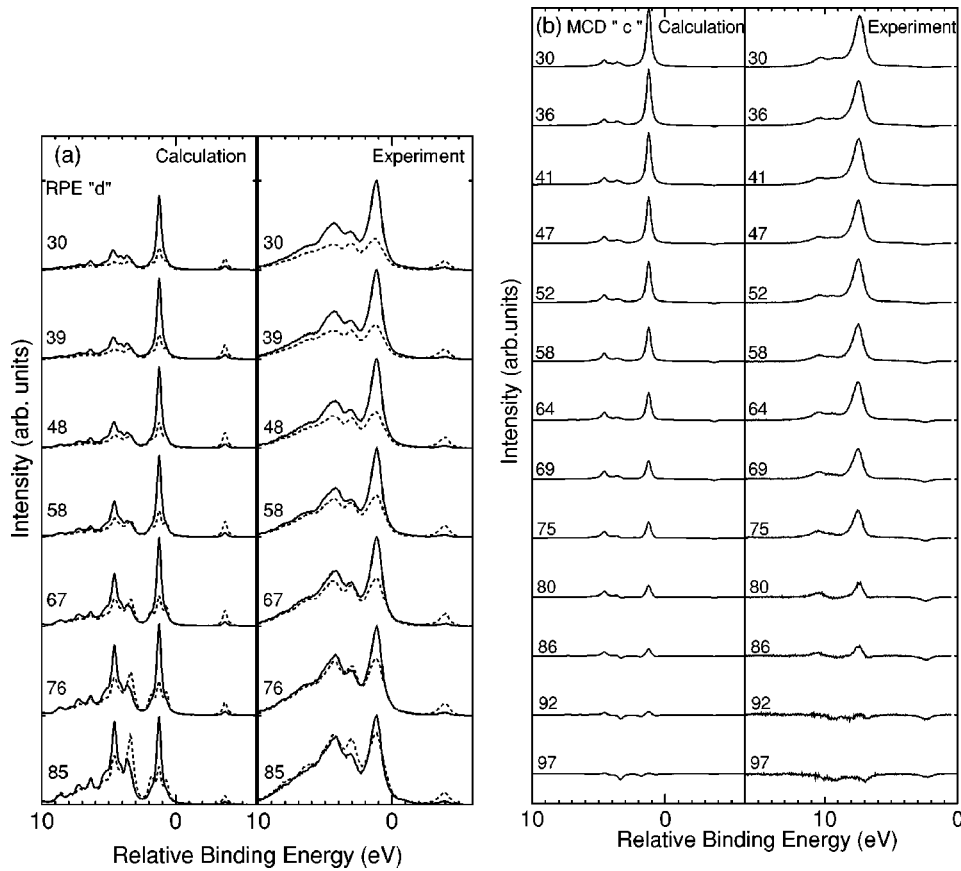
FIG. 7. Tb $3d \rightarrow 4f$ RPE at different angles for $h\nu = d$. The geometry is as in Fig. 1(b) with p_{in} indicated for each spectrum. (a) RPE for $+$ helicity (drawn line) and $-$ helicity (dashed line); (b) resulting MCD. Left panels: calculation; right panels: experimental results.

spin-up $4f$ states are filled while the spin-down $4f$ states contain only one electron.

We also presented theoretical results for angle dependence of the RPE and its MCD in the M_5 region. The calculated results with the photon energy above the M_5 threshold have been compared with the experimental results and show good agreement. Interestingly, there is a very strong angle dependence of the spectral shape which can be used to obtain extra information. For a system with a known ground state, information can be obtained on the phase factors of the outgoing photoelectron and on the angular dependence of the intra-atomic Coulomb interaction. Vice versa, when we know these atom-specific parameters, e.g., from Hartree-Fock calculations, we could use the angle dependence to obtain information about the ground-state properties of the system, much along the lines of the sum-rule analysis for second-order processes.[4,6,12,14]

[1] B.T. Thole, P. Carra, F. Sette, and G. van der Laan, Phys. Rev. Lett. **68**, 1943 (1992).

[2] P. Carra, B.T. Thole, M. Altarelli, and X. Wang, Phys. Rev. Lett. **70**, 694 (1993).

[3] G. van der Laan, Phys. Rev. B **57**, 112 (1998).

[4] B.T. Thole, H.A. Dürr, and G. van der Laan, Phys. Rev. Lett. **74**, 2371 (1995).

[5] L. Braicovich, G. van der Laan, G. Ghiringhelli, A. Tagliaferri, M.A. van Veenendaal, N.B. Brookes, M.M. Chervinskii, C. Dallera, B. De Michelis, and H.A. Dürr, Phys. Rev. Lett. **82**, 1566 (1999).

[6] L. Braicovich, A. Tagliaferri, G. van der Laan, G. Ghiringhelli, and N.B. Brookes, Phys. Rev. Lett. **90**, 117401 (2003).

[7] K. Fukui, H. Ogasawara, A. Kotani, T. Iwazumi, H. Shoji, and T. Nakamura, J. Phys. Soc. Jpn. **70**, 1230 (2001).

[8] H.A. Dürr, G. van der Laan, and M. Surman, J. Phys.: Condens. Matter **8**, L7 (1996).

[9] G. van der Laan, H.A. Dürr, and M. Surman, J. Electron Spectrosc. Relat. Phenom. **78**, 213 (1996).

[10] H.A. Dürr, G. van der Laan, D. Spanke, F.U. Hillebrecht, and N.B. Brookes, Europhys. Lett. **40**, 171 (1997).

[11] H.A. Dürr, G. van der Laan, D. Spanke, F.U. Hillebrecht, and N.B. Brookes, J. Electron Spectrosc. Relat. Phenom. **93**, 233 (1998).

[12] G. van der Laan and B.T. Thole, J. Phys.: Condens. Matter **7**, 9947 (1995).

[13] M. Taguchi and G. van der Laan, Phys. Rev. B **66**, 140401(R) (2002).

[14] M. van Veenendaal, P. Carra, and B.T. Thole, Phys. Rev. B **54**, 16 010 (1996).

[15] G. van der Laan and B.T. Thole, Phys. Rev. Lett. **60**, 1977 (1988).

[16] G. van der Laan, Phys. Rev. Lett. **82**, 640 (1999).

[17] B.T. Thole, G. van der Laan, J.C. Fuggle, G.A. Sawatzky, R.C. Karnatak, and J.M. Esteva, Phys. Rev. B **32**, 5107 (1985).

[18] G. van der Laan and B.T. Thole, Phys. Rev. B **48**, 210 (1993).

[19] G. van der Laan, E. Arenholz, Z. Hu, A. Bauer, E. Weschke, Ch. Schüssler-Langeheine, E. Navas, A. Mühlig, G. Kaindl, J.B. Goedkoop, and N.B. Brookes, Phys. Rev. B **59**, 8835 (1999).

[20] G. van der Laan, B.T. Thole, G.A. Sawatzky, J.B. Goedkoop, J.C. Fuggle, J.M. Esteva, R. Karnatak, J.P. Remeika, and H.A. Dabkowska, Phys. Rev. B **34**, 6529 (1986).

[21] G. van der Laan, E. Arenholz, E. Navas, A. Bauer, and G. Kaindl, Phys. Rev. B **53**, R5998 (1996).

[22] E. Arenholz, E. Navas, K. Starke, L. Baumgarten, and G. Kaindl, Phys. Rev. B **51**, 8211 (1995).

[23] Y. Ufuktepe, S. Kimura, T. Kinoshita, K.G. Nath, H. Kumigashira, T. Takahashi, T. Matsumura, T. Suzuki, H. Ogasawara, and A. Kotani, J. Phys. Soc. Jpn. **67**, 2018 (1998).

[24] E.U. Condon and G.H. Shortley, *The Theory of Atomic Spectra* (Cambridge University Press, Cambridge, 1959).

[25] R.D. Cowan, *The Theory of Atomic Structure and Spectra* (University of California Press, Berkeley, 1981).

[26] G. van der Laan and B.T. Thole, Phys. Rev. B **48**, 210 (1993).

[27] G. van der Laan, E. Arenholz, E. Navas, Z. Hu, E. Mentz, A. Bauer, and G. Kaindl, Phys. Rev. B **56**, 3244 (1997).

[28] N.B. Brookes, G. Ghiringhelli, O. Tjernberg, L.H. Tjeng, T. Mizokawa, T.W. Li, and A.A. Menovsky, Phys. Rev. Lett. **87**, 237003 (2001).